

Controllable microwave frequency comb generation in a tunable superconducting coplanar-waveguide resonator

Shuai-Peng Wang(王帅鹏), Zhen Chen(陈臻), and Tiefu Li(李铁夫)

Citation: Chin. Phys. B, 2021, 30 (**4**): 048501. DOI: 10.1088/1674-1056/abc2bb
Journal homepage: http://cpb.iphy.ac.cn; http://iopscience.iop.org/cpb

What follows is a list of articles you may be interested in

Micro-scale photon source in a hybrid cQED system

Ming-Bo Chen(陈明博), Bao-Chuan Wang(王保传), Si-Si Gu(顾思思), Ting Lin(林霆), Hai-Ou Li(李海欧), Gang Cao(曹刚)†, and Guo-Ping Guo(郭国平)‡

Chin. Phys. B, 2021, 30 (**4**): 048507. DOI: 10.1088/1674-1056/abe29b

Characterization of barrier-tunable radio-frequency-SQUID for Maxwell's demon experiment

Gang Li(李刚), Suman Dhamala, Hao Li(李浩), Jian-She Liu(刘建设), Wei Chen(陈炜)

Chin. Phys. B, 2018, 27 (**6**): 068501. DOI: 10.1088/1674-1056/27/6/068501

Modulation depth of series SQUIDs modified by Josephson junction area

Jie Liu(刘杰), He Gao(高鹤), Gang Li(李刚), Zheng Wei Li(李正伟), Kamal Ahmada, Zhang Ying Shan(张颖珊), Jian She Liu(刘建设), Wei Chen(陈炜)

Chin. Phys. B, 2017, 26 (**9**): 098501. DOI: 10.1088/1674-1056/26/9/098501

An efficient calibration method for SQUID measurement system using three orthogonal Helmholtz coils

Hua Li(李华), Shu-Lin Zhang(张树林), Chao-Xiang Zhang(张朝祥), Xiang-Yan Kong(孔祥燕), Xiao-Ming Xie(谢晓明)

Chin. Phys. B, 2016, 25 (**6**): 068501. DOI: 10.1088/1674-1056/25/6/068501

Low-T_c direct current superconducting quantum interference device magnetometer-based 36-channel magnetocardiography system in a magnetically shielded room

Qiu Yang, Li Hua, Zhang Shu-Lin, Wang Yong-Liang, Kong Xiang-Yan, Zhang Chao-Xiang, Zhang Yong-Sheng, Xu Xiao-Feng, Yang Kang, Xie Xiao-Ming

Chin. Phys. B, 2015, 24 (**7**): 078501. DOI: 10.1088/1674-1056/24/7/078501

Controllable microwave frequency comb generation in a tunable superconducting coplanar-waveguide resonator*

Shuai-Peng Wang(王帅鹏)[1], Zhen Chen(陈臻)[1,3], and Tiefu Li(李铁夫)[2,1,3,4,†]

[1] *Quantum Physics and Quantum Information Division, Beijing Computational Science Research Center, Beijing* 100193, *China*
[2] *Institute of Microelectronics, Tsinghua University, Beijing* 100084, *China*
[3] *Beijing Academy of Quantum Information Sciences, Beijing* 100193, *China*
[4] *Frontier Science Center for Quantum Information, Beijing* 100084, *China*

(Received 19 August 2020; revised manuscript received 18 September 2020; accepted manuscript online 20 October 2020)

Frequency combs are useful in a wide range of applications, such as optical metrology and high-precision spectroscopy. We experimentally study a controllable frequency comb generated in a tunable superconducting coplanar-waveguide resonator in the microwave regime. A two-tone drive is applied on one of the resonance modes of the resonator and comb generation is observed around the resonance frequency of the resonator. Both central frequency and teeth density of the comb are precisely controllable, and the teeth spacing can be adjusted from Hz to MHz. Moreover, we show that a few hundreds of sidebands can be generated using a sufficiently strong drive power and the weakest drive power needed to generate the comb can be reduced to approach the quantum limit. These experimental results can be qualitatively explained via theoretical analysis.

Keywords: superconducting circuit, SQUID, microwave frequency comb

PACS: 85.25.Am, 85.25.Cp, 85.25.Dq **DOI:** 10.1088/1674-1056/abc2bb

1. Introduction

Optical frequency combs[1,2] have attracted much attention because of their usefulness in a wide range of applications, including optical clocks,[3] spectroscopy,[4,5] frequency metrology,[6] and ultrastable microwave generation.[7] The conventional method to generate frequency combs is to use mode-locked femtosecond lasers.[1,2] An alternative and more versatile and compact way is based on high-Q microresonators.[8–11] The frequency combs related to the latter method is also called Kerr combs because the method exploits the Kerr nonlinearity of the material medium of the microresonator. The corresponding comb-generating mechanism can be described as a cascade of degenerate and nondegenerate four-wave mixing.[8] Even though the basic idea is simple, both theoretical analysis and numerical simulation can however be quite complicated because it involves the interaction of a strong drive with hundreds of modes of the microresonator.

Recently, microwave Kerr comb generation[12,13] was observed in a superconducting coplanar-waveguide resonator where the kinetic inductance of the superconducting material provides the nonlinearity.[12] This method implies more direct measurements with relatively simple instrumentation for studying Kerr combs. Here we introduce an alternative design for generating microwave Kerr combs. We use a $\lambda/2$-type superconducting coplanar-waveguide resonator embedded with a superconducting quantum interference device (SQUID).[14,15] The same kind of devices are also typically used as quantum-limited amplifiers[16–18] in the area of superconducting quantum information processing. This SQUID can offer a strong nonlinearity to the coplanar-waveguide resonator. In our experiment, a two-tone drive[19] is applied on one of the resonance modes of the resonator. Comb generation is observed around the resonance frequency of the resonator, with the teeth spacing exactly equal to the frequency difference between the two drive tones applied.

2. Experiment and analysis

The device structure is similar to that in Refs. [20,21] except that the flux-qubit loop is replaced by a SQUID loop. The superconducting coplanar-waveguide resonator is made by patterning a niobium thin film of thickness 50 nm deposited on a 10×3 mm^2 silicon chip via electron beam lithography. The width of the central conductor is 20 μm separated from the lateral ground planes extending to the edges of the chip by a gap of width 11.5 μm resulting in an impedance $Z = 50$ Ω, so as to be optimally matched to the conventional microwave components. Here we use a meandering coplanar waveguide of length $l = 24$ mm for the resonator [see Fig. 1(a)]. This coplanar-waveguide resonator is coupled to a feed line (used for input or output port) via an interdigitated capacitor of ∼15 fF at each end of the resonator, fanning out to the edge

*Project supported by the Science Challenge Project (Grant No. TZ2018003), the National Key Research and Development Program of China (Grant No. 2016YFA0301200), the National Natural Science Foundation of China (Grant Nos. 62074091, 11934010, U1801661, and U1930402), and the BAQIS Research Program (Grant No. Y18G27).

†Corresponding author. E-mail: litf@tsinghua.edu.cn

© 2021 Chinese Physical Society and IOP Publishing Ltd

of the chip and keeping the impedance constant [see Fig. 1(b)]. The SQUID loop is also fabricated on the silicon substrate in the middle of the central conductor of the coplanar-waveguide resonator by using both the electron beam lithography and the double-angle evaporation of aluminium, with a critical current $I_c \sim 1.5$ μA achieved for each of the two Josephson junctions in the SQUID [see Fig. 1(c)].[22,23] An external magnetic field generated by a magnetic coil surrounding the device is applied to tune the magnetic flux threading through the SQUID loop to vary the effective inductance of the SQUID, so as to change the resonance frequency of the resonator (see Fig. 2).

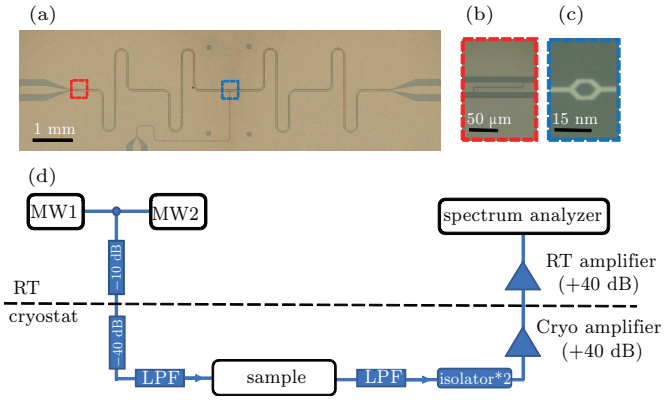


Fig. 1. (a) Optical image of the superconducting coplanar-waveguide resonator embedded with a SQUID. (b) Optical image of the coupling capacitor at the left end of the resonator, as indicated by the red rectangle area in panel (a). (c) Optical image of the SQUID loop, as indicated by the blue rectangle area in panel (a). (d) Schematic of the experimental setup, where MW1 and MW2 are two microwave generators and LPF is a 12 GHz low pass filter.

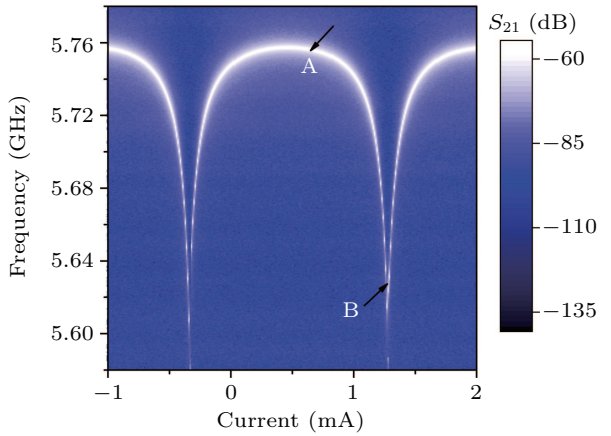


Fig. 2. Transmission spectrum of the λ mode of the resonator versus the current applied to the magnetic coil surrounding the device. The black arrows indicate the two bias points (A and B) chosen for the following experiment.

The whole device is placed in the sample chamber of the dilution refrigerator, which is cooled down to a temperature near 20 mK. The two-tone drive is generated by two separate microwave generators at room temperature. The drive frequency is on resonance with the λ mode of the resonator in Figs. 3, 4 and 6, and on resonance with the $\lambda/2$ mode of the resonator in Fig. 6. The drive signals transmit through a series of attenuators anchored at different stages in the dilution refrigerator before finally reaching the device. The output signals are collected by a spectrum analyzer at room temperature after two stages of isolations and amplifications [see Fig. 1(d)].

Beating between the two strong drive tones results in a broadband of sidebands generated around them. The linewidths of the sidebands are extremely narrow and cannot be directly resolved with the spectrum analyzer. The frequency spacing between the nearest-neighbor sidebands, i.e., the teeth spacing, is precisely equal to the frequency difference between the two drive tones, $\Delta f = f_{d2} - f_{d1}$. The teeth spacing can be adjusted from Hz to MHz, as shown in Fig. 3.

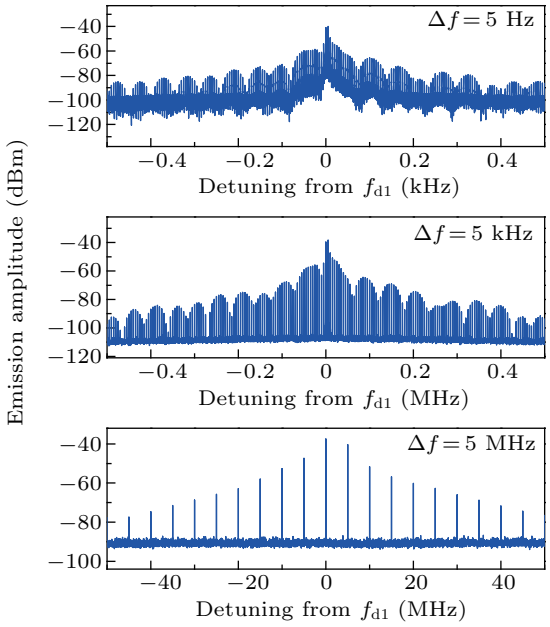


Fig. 3. Comb generation with tunable teeth density. The frequency of one drive tone is fixed at $f_{d1} = 5.757$ GHz (indicated by the bias point A in Fig. 2) and the frequency of another drive tone is given as $f_{d2} = f_{d1} + 5$ Hz, 5 kHz, and 5 MHz, respectively.

The overall profile of the comb depends on the power of the drive tone applied to the coplanar-waveguide resonator. As the drive power increases, the comb profile demonstrates different characteristic features. We find that there are three different regimes according to the profile shape. When the drive power is weak, the amplitudes of the high-order sidebands decrease linearly, with the comb profile exhibiting a triangle-like shape (see the results in Fig. 4 when the drive power is −70 dBm and −65 dBm, respectively). When the drive power is very strong, the comb profile spreads and exhibits a complicated periodic structure, with the bandwidth of the whole comb extending significantly (see the results in Fig. 4 when the drive power is −50 dBm and −40 dBm, respectively). In the intermediate regime, the emission background protrudes and becomes a continuous peak in the frequency spectrum near the drive tones (see the results in Fig. 4 when the drive power is −64 dBm and −63 dBm, respectively). In our experiment, the protuberance of the emission background is a signature predicting the occurrence of the comb-bandwidth broadening and

the appearance of the complicated periodic structure, whereas it gradually vanishes with increasing drive power.

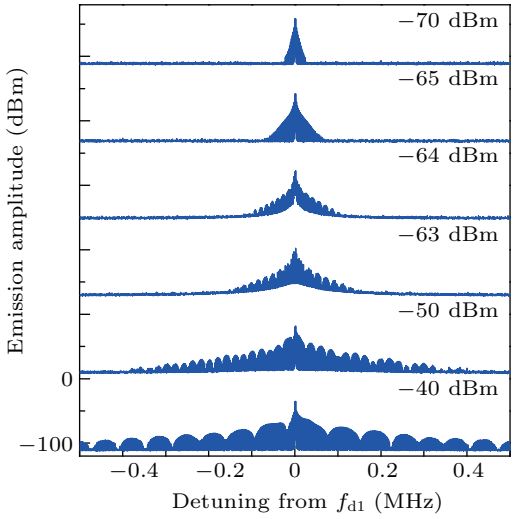


Fig. 4. Power dependence of the comb profile. The frequencies of the two drive tones are $f_{d1} = 5.757$ GHz and $f_{d2} = f_{d1} + 2$ kHz (indicated by the bias point A in Fig. 2), respectively. Drive powers applied at the device input port are −60 dBm, −55 dBm, −54 dBm, −53 dBm, −40 dBm, and −30 dBm, respectively. Traces are offset vertically for clarity.

The driven superconducting coplanar-waveguide resonator embedded with the SQUID can be described by the following nonlinear equation:[24]

$$\frac{1}{(2\pi f_0)^2}\frac{\mathrm{d}^2\Phi}{\mathrm{d}t^2}+\frac{1}{2\pi f_0 Q}\frac{\mathrm{d}\Phi}{\mathrm{d}t}+\Phi+\sum_{n=2}^{N} g_n\Phi^n=\Phi_{\mathrm{drive}}(t), \quad (1)$$

where Φ is the flux associated with the voltage at one end of the transmission line $V = \mathrm{d}\Phi/\mathrm{d}t$, f_0 and Q are the bare resonance frequency and quality factor, respectively, and g_n is the coefficient related to the nth-order nonlinearity. A two-tone drive gives correction terms

$$g_n[A_{\mathrm{d1}}\,\mathrm{e}^{\mathrm{i}\pi f_{\mathrm{d1}}t}+A_{\mathrm{d2}}\,\mathrm{e}^{\mathrm{i}\pi f_{\mathrm{d2}}t}]^n \quad (2)$$

to the linear response of the resonator. Comb sidebands are just the intermodulation products of the drive tones resulting from the expansion of the binomial in the following equation:

$$f_{\mathrm{IMP}} = n_{\mathrm{d1}}f_{\mathrm{d1}} + n_{\mathrm{d2}}f_{\mathrm{d2}}, \quad (3)$$

where n_{d1} and n_{d2} are arbitrary integers. Because of the Josephson effects, the nonlinearity introduced by the SQUID embedded in the coplanar-waveguide resonator has a current-flux relation, $\mathrm{i}(\Phi) = -\mathrm{i}(-\Phi)$, which is an odd function. It means that only the odd powers of Φ are nonzero in Eq. (1). This conclusion is consistent with our experimental results in Figs. 3 and 4, where only the odd-order intermodulation products (e.g., $2f_{\mathrm{d1}} \pm f_{\mathrm{d2}}$, $2f_{\mathrm{d2}} \pm f_{\mathrm{d1}}$, $3f_{\mathrm{d1}} \pm 2f_{\mathrm{d2}}$, $3f_{\mathrm{d2}} \pm 2f_{\mathrm{d1}}$, etc.) are observed in the spectra.

Following the above analysis, it is also possible to observe the comb generation at the odd-number modes simultaneously. For example, if f_{d1} is on resonance with the $n\lambda/2$ mode of the resonator, n will be an odd integer, then $2f_{\mathrm{d1}} - f_{\mathrm{d2}}$, $2f_{\mathrm{d2}} - f_{\mathrm{d1}}$, $3f_{\mathrm{d1}} - 2f_{\mathrm{d2}}$, $3f_{\mathrm{d2}} - 2f_{\mathrm{d1}}, \ldots$ are near the $n\lambda/2$ mode, $2f_{\mathrm{d1}} + f_{\mathrm{d2}}$, $2f_{\mathrm{d2}} + 2f_{\mathrm{d1}}$, $4f_{\mathrm{d1}} - f_{\mathrm{d2}}$, $4f_{\mathrm{d2}} - f_{\mathrm{d1}}, \ldots$ are near the $3n\lambda/2$ mode, and the same for higher odd-number modes. A simple numerical simulation result of the comb generation is presented in Fig. 5. We can see clearly that the comb can be generated at the odd-number modes simultaneously even when only the lowest odd-nonlinear coefficient g_3 is considered. We also experimentally observe the comb generation at the $\lambda/2$ and $3\lambda/2$ modes simultaneously when applying the two-tone drive on resonance with the $\lambda/2$ mode of the resonator. The results are shown in Fig. 6. Because of the limitation of the measurement bandwidth in our experiment, we can only observe the lowest two odd-number modes of the resonator. It is worth pointing out that if we want to get a more faithful simulation of the experimental results especially when the drive power is very strong and the number of the sidebands is large, the knowledge of the nonlinear coefficient $g(n)$ as a function of n will be necessary,[19] however it is hard to determine $g(n)$ by the experiment. Further theoretical work may be needed to solve this problem.

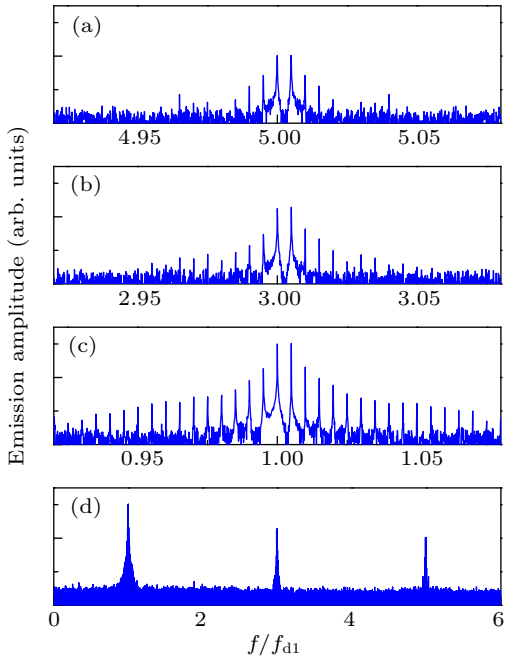


Fig. 5. Numerical simulation of the comb generation. Here (a), (b), (c) are enlarged views of the spectrum in (c) near $5f_{\mathrm{d1}}$, $3f_{\mathrm{d1}}$, f_{d1}, respectively. To simulate the comb generation, Eq. (1) with $\Phi_{\mathrm{drive}}(t) = \mathrm{A}[\cos(2\pi f_{\mathrm{d1}}t) + \cos(2\pi f_{\mathrm{d2}}t)]$ is numerically solved and the output is sampled appropriately and fast Fourier transformed to get the intermodulation spectrum. For simplicity, only the lowest odd nonlinear coefficient g_3 is considered. In the simulation, $f_{\mathrm{d1}} = f_0$ is assumed to be unity and the other parameters are $g_3 = 0.1$, $Q = 2800$, $\Delta f = 0.005$, and $A = 50$.

The strength of the nonlinearity introduced by the SQUID is related to the slope of the curve in the transmission spectrum of the resonator modulated by the external magnetic field and reaches the maximum at the dip where the slope is largest[25] (see Fig. 2). Therefore, when tune the resonance frequency

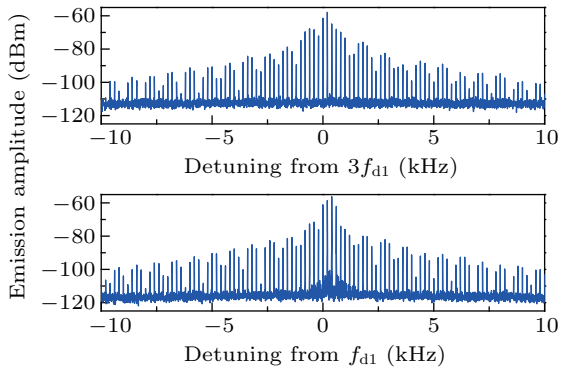


Fig. 6. Comb generation at the $\lambda/2$ and $3\lambda/2$ modes of the resonator simultaneously. The frequencies of the two drive tones are $f_{d1} = 2.872$ GHz and $f_{d2} = f_{d1} + 0.2$ kHz, respectively. Drive powers applied at the device input port are -60 dBm.

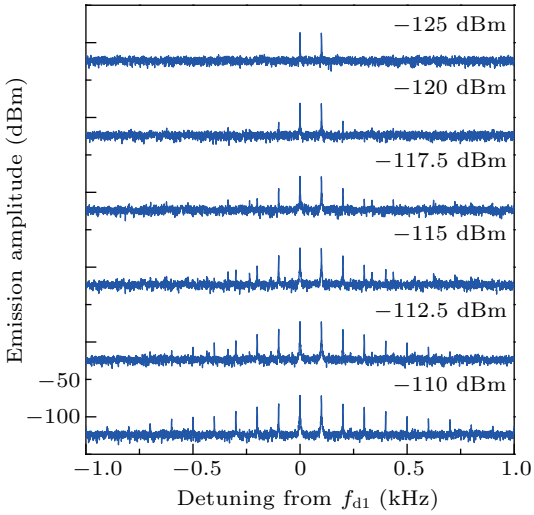


Fig. 7. Comb generation in the weak drive-power limit. The frequencies of the two drive tones are $f_{d1} = 5.629$ GHz and $f_{d2} = f_{d1} + 0.1$ kHz (indicated by the bias point B in Fig. 2), respectively. Drive powers applied at the device input port are -125 dBm, -120 dBm, -117.5 dBm, -115 dBm, -112.5 dBm, and -110 dBm, respectively. The corresponding average photon number in the resonator for each drive frequency is about 1.2, 8.3, 10.4, 11.9, 13.1, and 14.0, respectively. Traces are offset vertically for clarity.

of the resonator to the dip (indicated by the bias point B in Fig. 2), it can be expected that the needed drive power to generate the comb is much lower compared with the cases when the resonance frequency of the resonator is at the top (indicated by the bias point A in Fig. 2). The results of the comb generation in the weak drive-power limit are shown in the Fig. 7. We can evaluate if the weak drive power is approaching the quantum limit by calculating the average number of photons in the resonator that come from the driving field, which is given by

$$\bar{n}_{\mathrm{d}} = \frac{P_{\mathrm{d}}}{\hbar\kappa\omega_{\mathrm{r}}}, \tag{4}$$

where $\kappa = 1.8$ MHz is the total loss rate of the resonator, ω_{r} is the resonance frequency of the resonator, and P_{d} is the drive power. We can see that (the results in Fig. 6 when the drive power is -120 dBm and -117.5 dBm, respectively), in the weak drive-power limit, the average photon number in the resonator for each drive frequency is only $\sim$10 when the nearest sidebands start to be generated around drive tones. When replace the junctions in the SQUID with smaller junctions, we can further increase the strength of the nonlinearity and possibly observe the comb generation in the quantum limit, i.e., at the single-photon level. Owing to the tunability of the SQUID inductance, our setup provides an on-chip device to implement controllable frequency comb generation.

3. Conclusion

In summary, we have fabricated a tunable superconducting coplanar-waveguide resonator with strong nonlinearity resulting from the SQUID embedded and also demonstrated its nonlinear effects under a strong or weak two-tone drive. In our experiment, a few hundreds of sidebands are generated when the applied drive power is sufficiently strong, forming a frequency comb with different profiles, and the weakest drive power needed to generate the comb can be reduced to approach the quantum limit. The central frequency of the comb can be tuned along with the resonance frequency of the resonator by varying the magnetic flux threading through the SQUID loop. Also, we find that the teeth density of the comb is precisely controllable via the frequency difference of the two applied drive tones. Because of its simple architecture and flexible parameters, our device offers an ideal platform to study Kerr combs in the microwave regime. Further improvements may include the integration of a SQUID array in the coplanar-waveguide resonator to enhance the frequency tunability and meanwhile to achieve a larger dynamic range.[26,27]

References

[1] Udem T, Holzwarth R and Hansch T W 2002 *Nature* **416** 233
[2] Cundiff S T and Ye J 2003 *Rev. Mod. Phys.* **75** 325
[3] Chou C W, Hume D B, Koelemeij J C J, Wineland D J and Rosenband T 2010 *Phys. Rev. Lett.* **104** 070802
[4] Thorpe M J, Moll K D, Jones J J, Safdi B and Ye J 2006 *Science* **311** 1595
[5] Diddams S A, Hollberg L and Mbele V 2007 *Nature* **445** 627
[6] Coddington I, Swann W C, Nenadovic L and Newbury N R 2009 *Nat. Photon.* **3** 351
[7] Fortier T M, Kirchner M S, Quinlan F, Taylor J, Bergquist J C, Rosenband T, Lemke N, Ludlow A, Jiang Y, Oates C W and Diddams S A 2011 *Nat. Photon.* **5** 425
[8] Del'Haye P, Schliesser A, Arcizet O, Wilken T, Holzwarth R and Kippenberg T J 2007 *Nature* **450** 1214
[9] Kippenberg T J, Holzwarth R, Diddams S A 2011 *Science* **332** 555
[10] Griffith A G, Lau R K W, Cardenas J, Okawachi Y, Mohanty A, Fain R, Lee Y H D, Yu M, Phare C T, Poitras C B, Gaeta A L and Lipson M 2015 *Nat. Commun.* **6** 6299
[11] Liang W, Eliyahu D, Ilchenko V S, Savchenkov A A, Matsko A B, Seide D and Maleki L 2015 *Nat. Commun.* **6** 7957
[12] Erickson R P, Vissers M R, Sandberg M, Jefferts S R and Pappas D P 2014 *Phys. Rev. Lett.* **113** 187002
[13] Solinas P, Gasparinetti S, Golubev D and Giazotto F 2015 *Sci. Rep.* **5** 12260
[14] Sandberg M, Wilson C M, Persson F, Bauch T, Johansson G, Shumeiko V 2008 *Appl. Phys. Lett.* **92** 203501
[15] Wilson C M, Duty T, Sandberg M, Persson F, Shumeiko V and Delsing P 2010 *Phys. Rev. Lett.* **105** 233907
[16] Yamamoto T, Inomata K, Watanabe M, Matsuba K, Miyazaki T, Oliver W D, Nakamura Y and Tsai J S 2008 *Appl. Phys. Lett.* **93** 042510

[17] Huang K, Guo Q, Song C, Zheng Y, Deng H, Wu Y, Jin Y, Zhu X and Zheng D 2017 *Chin. Phys. B* **26** 094203
[18] Su F F, Wang Z T, Xu H K, Zhao S, Yan H, Yang Z H, Tian Y, Zhao S P 2019 *Chin. Phys. B* **28** 110303
[19] Hutter C, Platz D, Tholén E A, Hansson T H and Haviland D B 2010 *Phys. Rev. Lett.* **104** 050801
[20] Chen Z, Wang Y, Li T, Tian L, Qiu Y, Inomata K, Yoshihara F, Han S, Nori F, Tsai J S and You J Q 2017 *Phys. Rev. A* **96** 012325
[21] Wang S P, Zhang G Q, Wang Y, Chen Z, Li T, Tsai J S, Zhu S Y and You J Q 2020 *Phys. Rev. Appl.* **13** 054063
[22] Wu Y L, Deng H, Yu H F, Xue G M, Tian Y, Li J, Chen Y F, Zhao S P and Zheng D N 2013 *Chin. Phys. B* **22** 060309
[23] Zhang K, Li M M, Liu Q, Yu H F and Yu Y 2017 *Chin. Phys. B* **26** 078501
[24] Tholén E A, Ergül A, Schaeffer D and Haviland D B 2014 *EPJ Quantum Technol.* **1** 5
[25] Krantz P, Reshitnyk Y, Wustmann W, Bylander J, Gustavsson S, Oliver W D, Duty T, Shumeiko V and Delsing P 2013 *New J. Phys.* **15** 105002
[26] Eichler C and Wallraf A 2014 *EPJ Quantum Technol.* **1** 2
[27] Tancredi G, Ithier G and Meeson P J 2013 *Appl. Phys. Lett.* **103** 063504